

See discussions, stats, and author profiles for this publication at: <https://www.researchgate.net/publication/264628350>

# Electron Spin Resonance of Nitrogen–Vacancy Defects Embedded in Single Nanodiamonds in an ABEL Trap

ARTICLE *in* NANO LETTERS · AUGUST 2014

Impact Factor: 13.59 · DOI: 10.1021/nl5023964 · Source: PubMed

---

CITATION

1

READS

50

## 3 AUTHORS, INCLUDING:



Metin Kayci

École Polytechnique Fédérale de Lausanne

3 PUBLICATIONS 343 CITATIONS

[SEE PROFILE](#)



Aleksandra Radenovic

École Polytechnique Fédérale de Lausanne

68 PUBLICATIONS 4,069 CITATIONS

[SEE PROFILE](#)

# Electron Spin Resonance of Nitrogen-Vacancy Defects Embedded in Single Nanodiamonds in an ABEL Trap

Metin Kayci,<sup>\*,†</sup> Huan-Cheng Chang,<sup>‡</sup> and Aleksandra Radenovic<sup>†</sup>

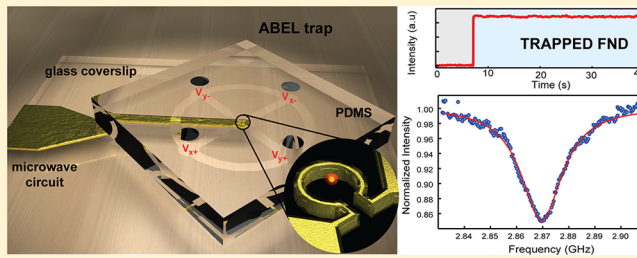
<sup>†</sup>Institute of Bioengineering, Ecole Polytechnique Federale de Lausanne (EPFL), CH-1015 Lausanne, Switzerland

<sup>‡</sup>Institute of Atomic and Molecular Sciences, Academia Sinica, Taipei 106, Taiwan, Republic of China

## S Supporting Information

**ABSTRACT:** Room temperature optically detected magnetic resonance of a single quantum object with nanoscale position control is an outstanding challenge in many areas, particularly in the life sciences. We introduce a novel approach to control the nitrogen-vacancy (NV) centers hosted in a single fluorescent nanodiamond (FND) for which an anti-Brownian electrokinetic trap (ABEL) performs the position control and an integrated radiofrequency (RF) circuit provides enhanced magnetic flux density for ensemble spin-state control simultaneously. We demonstrate static magnetic field sensing in platforms compatible with ABEL trap. With the advances in the synthesis and functionalization of stable arbitrarily small FNDs, we foresee the use of our device for the trapping and manipulation of single molecular-sized FNDs in aqueous solution.

**KEYWORDS:** Anti-Brownian electrokinetic trap (ABEL), fluorescent nanodiamonds (FND), nitrogen-vacancy, nanophotonics, electron spin resonance (ESR)



The progress in fluorescence imaging is determined by our ability to create bioimaging probes that will not saturate, blink nor photobleach and should not be destructive or toxic. Recently, a novel probe in the form of fluorescence nanodiamonds (FNDs) has been introduced as an appealing alternative to fluorescent proteins and organic dyes. FNDs contain built-in fluorophores, most often in the form of the defects such as nitrogen-vacancy complexes (e.g., NV).<sup>1</sup> The NV defects are atom-like and form photoluminescent color centers, which render them exceptionally photostable.<sup>2</sup> Besides bioimaging applications, the NV defects in the nanodiamond lattice are promising candidates for quantum optics and nanoscale metrology. It is demonstrated that FND can be a stable single photon source<sup>3</sup> and an emitter system providing optically accessible spin qubits.<sup>4</sup> Recently, electric and magnetic field sensing,<sup>5–7</sup> thermal sensing,<sup>8,9</sup> and single photon microscopy<sup>10</sup> has been achieved using NV defects. In addition, a NV based magnetic sensor works under ambient conditions, and it is biocompatible, which makes it an excellent candidate for bioimaging. So far, precise spatial control of nanodiamonds has been achieved using various modalities of scanning probe techniques.<sup>5,6,10–12</sup> However, this practice is less suitable in closed fluidic environments such as the interiors of microfluidic channels. Laser tweezers present compelling alternative to precise nanopositioning of nanostructures, owing to their ability to act *in situ*, in closed aqueous chambers, and their potential applicability to a broad range of dielectric materials.<sup>13,14</sup> Indeed, laser tweezers have been recently successfully employed to detect electron spin resonance (ESR) of nitrogen-vacancy centers in ensemble FNDs<sup>15</sup> and single FNDs.<sup>16</sup> Although an

attractive alternative to scanning probe techniques, detection of the ESR of nitrogen-vacancy centers in a single FND remains challenging due to the inherent limitation of laser tweezers. The force employed by laser tweezers scales with the volume of the trapped object: for example, to trap a 10 nm object requires 6 orders of magnitude as much input power as to trap a 1  $\mu\text{m}$  object rendering the trapping of the objects smaller than 100 nm challenging since it requires high laser powers ( $\sim$ 150 mW)<sup>16</sup> and high viscosity (5 cP).<sup>17</sup> In addition, since the force arises through a second-order interaction of the trapped object with the applied electric or magnetic field, the field must first polarize the object, and then it can generate the force between the induced dipole and a gradient in the field. A further drawback of optical trapping technique is its lack of selectivity. Optical trap generates a potential minimum for polarizable objects. Any sufficiently large polarizable object will be attracted and will fall into this minimum and be trapped. Laser tweezers cannot be used in dense dispersions because the trap will become overfilled by particles.<sup>18</sup> Moreover, high powers of the trapping laser might be too invasive for live cell magnetometry applications.

Anti-Brownian electrokinetic (ABEL) trap is a novel nonperturbative technique<sup>19,20</sup> that allows trapping and manipulating single fluorescent molecules of solution phase. It operates by tracking the Brownian motion of single fluorescent particle in solution and applying a time-dependent

**Received:** June 26, 2014

**Revised:** July 23, 2014

**Published:** August 11, 2014



ACS Publications

© 2014 American Chemical Society

5335

dx.doi.org/10.1021/nl5023964 | Nano Lett. 2014, 14, 5335–5341

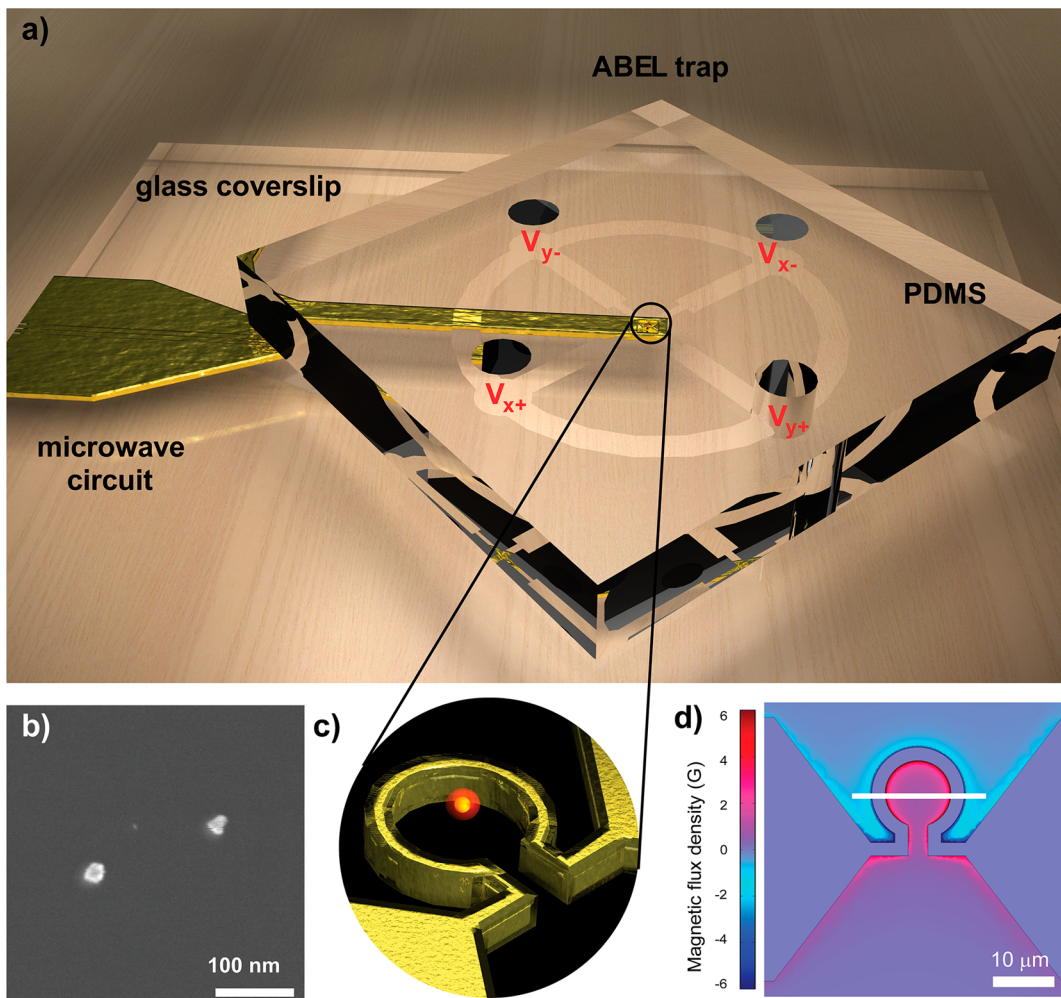


**Figure 1.** (a) Schematic of ABEL trap PDMS microfluidic cell with RF circuit integrated on the same glass coverslip. (b) SEM micrograph of 30 nm big fluorescent nanodiamonds. (c) Zoomed in trapping area shown in panel a indicating the relative location of FND in respect to the area with the enhanced homogeneous magnetic flux density. (d) Finite element analysis of the magnetic flux density in the discontinuity area of the coplanar waveguide when excited with a power of 20 dBm at 2.87 GHz.

electric field to induce an electrokinetic drift that cancels the Brownian motion. As the Brownian motion of different freely diffusing objects is uncorrelated; thus, the applied potential cannot cancel out more than a single molecule Brownian motion at a time, providing therefore required selectivity.<sup>21</sup> So far, ABEL trap has been used for trapping of DNA oligomers,<sup>22,23</sup> photosynthetic protein allophycocyanin (APC),<sup>24</sup> G-protein coupled receptors,<sup>25</sup> and even single organic dyes<sup>26,27</sup> with the photobleaching limited trapping period.

Here, we demonstrate an alternative scanning technique for magneto-optical spin detection under ambient and aqueous conditions by means of an ABEL trapping. Compared to the scanning techniques using embedded NV defects in a functionalized probe tip<sup>5,6,10–12</sup> ABEL trapping does not require a physical support and provides a new window into the complex fluidic environments. Using the ABEL trap, we control the position of a single nanodiamond particle containing NV defect centers at solution phase. As the NV defect has nonbleaching behavior the trap period is not limited by photobleaching, and in consequence, trapped FNDs can be localized to a very high precision. The near fields of an integrated RF circuit, together with a green laser, enable us to

excite the NV defects and change the spin-dependent luminescence intensity for electron spin resonance measurements.

**Results and Discussion.** ABEL trap performance significantly depends on the symmetry of the polydimethylsiloxane (PDMS) chamber,<sup>28</sup> and in our case, the trapping chamber had to be integrated with RF circuit, realized on the same cover-glass as shown in the schematics in Figure 1a,c. After finding the optimal PDMS trap geometry (see materials and methods), we have performed finite element analysis with an aim to test several RF circuits that will deliver relatively homogeneous magnetic flux density. As shown in Figure 1d, the chosen RF circuit delivers homogeneously magnetic field intensity of 1 G in the discontinuity area of the coplanar waveguide when excited with a frequency of 2.87 GHz at 20 dBm power. Prior to trapping measurements, we have characterized sonicated FNDs using scanning electron microscope (SEM). Although, many FNDs are still in aggregated form (data not shown) it is possible to find without difficulty numerous isolated FNDs as shown in the Figure 1b. ABEL trapping experiments were performed in a purpose-built optical setup detailed in Figure 2a, similar to one reported in refs 20 and 26. In our setup for single molecule fluorescence detection one can either use fast CMOS

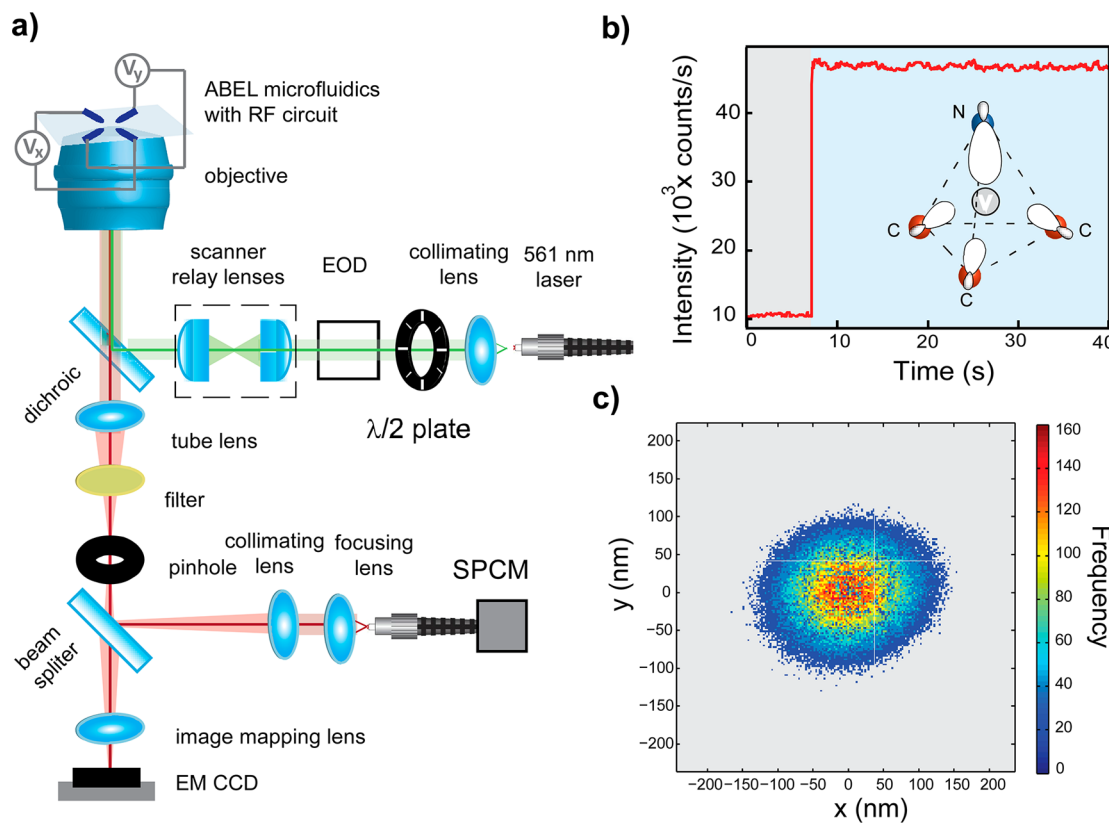


**Figure 2.** (a) Schematic of ABEL trap optic setup. The pair of electro optic deflectors (EODs) introduces an angle to the input beam with the voltage vector generated from the high voltage amplifier. The scanner relay lenses are coupling the angles to a position vector that forms the optic pattern in the sample plane. Confocal detection is performed with a pinhole placed in the first image plane. Beam splitter enables detection paths for camera and single photon counting module (SPCM). The filter implemented on the FPGA applies the feedback voltages to the high voltage amplifier based on the TLL pulse counts from the SPCM. (b) Fluorescence intensity profile of trapped and not trapped single FND; when the feedback is on (blue area of the graph) a single FND entering the target region is trapped. As the particle does not show photobleaching characteristics, it became trapped as long as the feedback is on. Inset shows lattice structure of the NV defect in FND. (c) Position histogram of the trapped FND.

(Neo Andor) camera, having feedback rate up to 400 Hz, or Avalanche Photodiode APD, having feedback rate up to 97.34 kHz; for details, see materials and methods. Before trapping, we investigated optimal laser scanning radius as shown in the Supporting Information Figure S1. To test the performance of our ABEL trap, we first trapped fluorescent 20 nm beads (fluospheres red–orange 580/605, F8786, Molecular Probes). We succeed in a trapping of these 20 nm fluorescent polystyrene beads for up to 20 s (see Supporting Information Figure S2a). Unsurprisingly, intensity profile indicates slow photobleaching of multiple fluorophores contained in a single 20 nm bead. In addition, ABEL trap performance was validated by cross-correlating positions measured using CMOS camera and positions extracted from the voltage vectors applied by the feedback using APD (Supporting Information Figure S2b).

After successful realization of the ABEL trap, we proceeded with trapping of 30 nm-sized single FNDs that contains approximately 10 NV defects (Figure 2b,c). The ABEL trapping, as for the 20 nm fluorescent beads, has been achieved through transversal electrokinetic forces generated in the microfluidics, while the out-of-plane movements are physically restricted by the trap cavity walls. The position deviation introduced by thermally driven Brownian motion is suppressed with the closed-loop feedback control system. High diffusion coefficient of the single FND requires a very fast position sensing scheme and feedback update that are not possible with

camera-based solutions. Although, as in the case of optical trapping we could increase viscosity<sup>16</sup> to allow camera-based detection for the trapping of single FNDs, having APD with feedback rate up to 97.34 kHz was not necessary. The position in the transverse plane is estimated via a Kalman filter implemented on a field-programmable gate array (FPGA) with a scanning Gaussian beam and confocal fluorescence signal detection on a single photon counting module (see materials and methods). The feedback voltages generating the electrokinetic forces are applied to orthogonal pairs of platinum electrodes integrated into the trap cell.

In the absence of the feedback, the 30 nm sized FNDs diffuse across the excitation pattern so fast that the contribution to the total fluorescence can be detected only by a detection system with the sub-millisecond temporal resolution. Thus, photons are counted through an avalanche photodiode (SPCM-AQRH-14, PerkinElmer) that generates a transistor-transistor logic (TLL) pulse train with 350 ps timing resolution. When the feedback was applied, only one of the diffusing FNDs was tracked and trapped to a submicron area (Figure 2c).

Feedback rate of 20 kHz<sup>20,26</sup> is sufficient to stably trap single 30 nm large FND for tens of minutes. In contrast to the intensity profile of single 20 nm fluorescent polystyrene bead, we observe no photobleaching (Figure 2b). Our observation is in accordance with previous results on the characterization of surface bound FNDs.<sup>29</sup> Electronic spin states of the NV defects

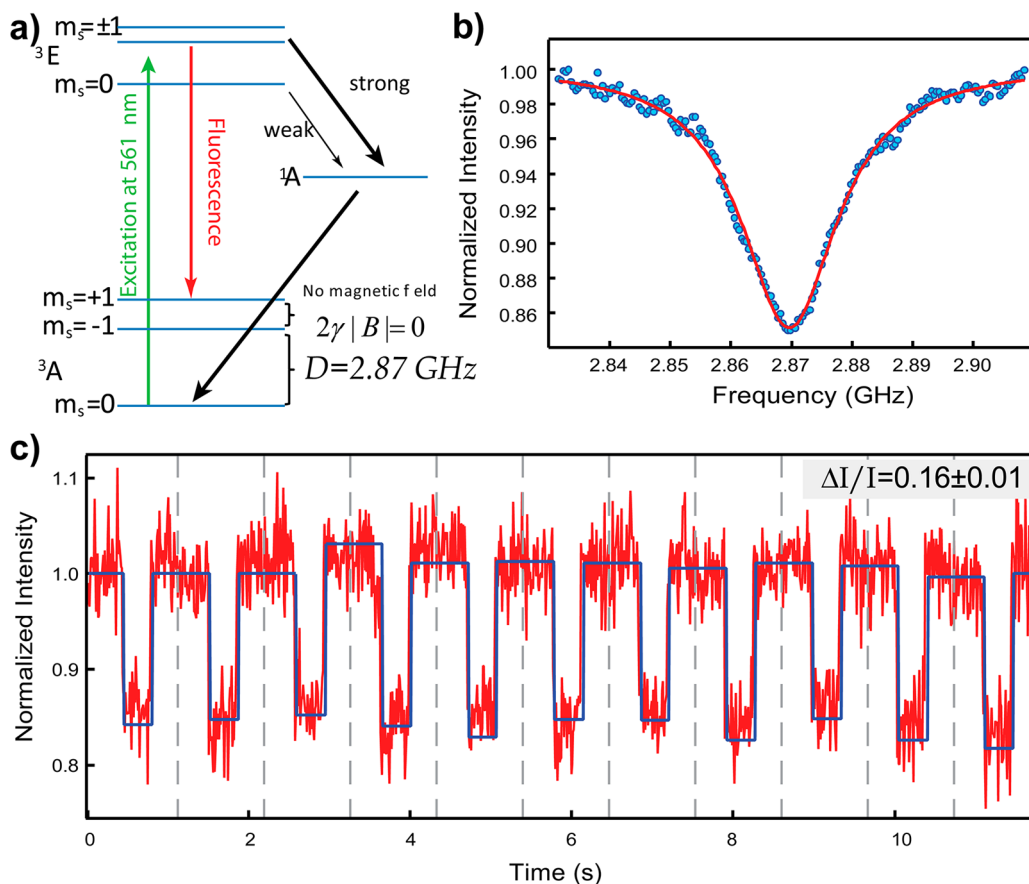


**Figure 3.** (a) Energy diagram of the ground state  $^3A$ , excited state  $^3E$ , and metastable singlet state  $^1A$  represented for NV. Dashed black arrows show the nonradiative decay via the singlet state. (b) ODMR spectra of NV defects in trapped FND. Microwave frequency swept in 1 MHz intervals of 10 ms dwell time. (c) Observation of the electron spin resonance at 2.87 GHz with 1:2 on/off microwave excitation. The dwell time was set to 200 ms.

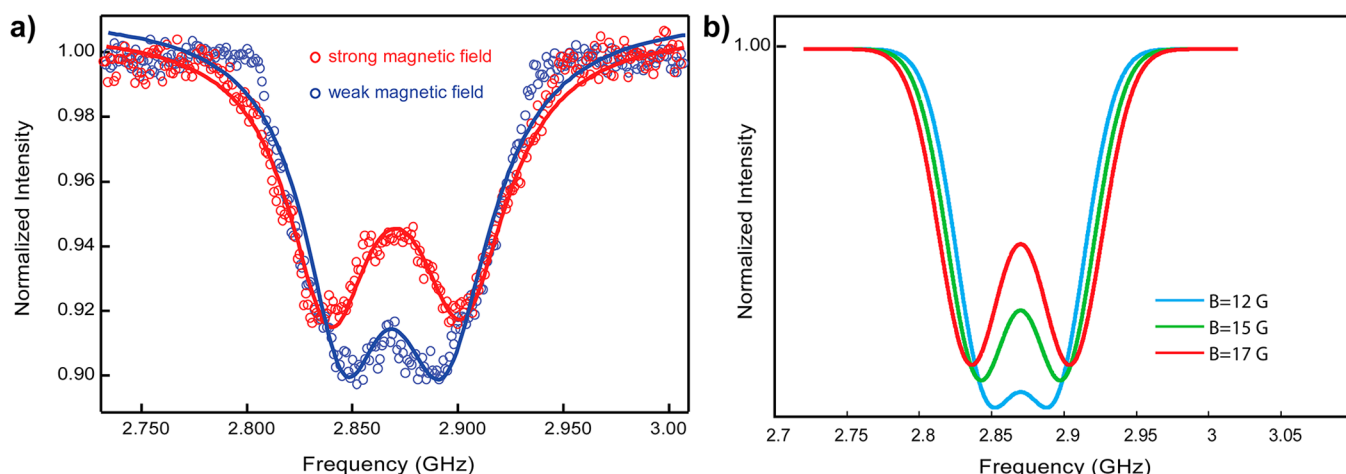


**Figure 4.** (a) Optically detected ESR spectra of an ABEL trapped single FND under presence of the weak and strong static magnetic field. The solid lines represent a two-Lorentzian fit defining transition frequencies. For the strong magnetic field we find  $f_{01} = 2838.7 \pm 0.385 \text{ MHz}$  and  $f_{02} = 2901.7 \pm 0.411 \text{ MHz}$ . While for the weak magnetic field we obtained  $f_{01} = 2844.7 \pm 0.665 \text{ MHz}$  and  $f_{02} = 2892 \pm 0.736 \text{ MHz}$ . The data points in the frequency sweep were acquired in steps of 1 MHz. (b) Modeled ESR spectra of rotationally diffusing single FND in ABEL trap at several magnetic field strengths. It is assumed the orientation of the particle acquires a random phase on each feedback step. By comparing the measured frequencies with our model, we can extract the values for the strong and weak magnetic fields ( $\sim 16$  and  $\sim 14 \text{ G}$ ).

in single FNDs were excited with the same laser,  $\lambda = 561 \text{ nm}$ , used for tracking. FND displacement distribution is shown in the form of 2d histogram (Figure 2c). Full width at half-maximum values for  $x$  and  $y$  dimensions,  $fwhm_x = 130 \text{ nm}$  and  $fwhm_y = 120 \text{ nm}$  have set our localization precisions for single

FND. Finally we showed that trapped single FNDs can be scanned over trap area using nanopositioning stage, which is integral part of our setup (see Supporting Information Movie).

Having in hand a method for manipulating, positioning, and characterizing single FNDs, we set out to perform ensemble

spin state control of the NV defects. This has been realized via an RF circuit patterned on a thin coverslip integrated to the ABEL trap microfluidics (Figure 1a) (see materials and methods). The engineered geometry of the discontinuity on the coplanar waveguide transmission line couples uniform oscillating magnetic fields to the NV defects over a 100  $\mu\text{m}$  area that can be used for scanning purposes in ABEL trap as well as other bioexperiments for bulk measurements. To probe the frequency-dependent coupling to the defects, a parametric sweep measurement with 1 MHz modulation and 10 ms dwell time was performed. The spin-dependent PL intensity of the NV defects has been collected with the same APD used for the position detection in ABEL trap. The photoluminescence drop around the resonance frequency showed a Lorentzian line shape, similar to the ones reported for the bulk measurements (Figure 3b). In addition, pulsed RF signal at the resonance frequency was applied with the extended dwell time, 200 ms (Figure 3c). Our results demonstrate that observation window at resonance could be extended to allow better estimation of the changes in the spin-dependent PL intensity.

The NV centers in ABEL trap are not fixed in orientation. Therefore, we modeled the ESR spectra of the particle exposed to the random rotational motion (see Supporting Information). Basically the “random walk” of the angle between the NV symmetry axis and the microscope objective, which is fixed with respect to the external magnetic field, leads to a change in the NV excitation level, the emitted fluorescence collection efficiency, and the strength of magnetic field component aligned with the spin orientation. The contributions of uncorrelated angles form the spectra with two broadened peaks split by a frequency that is dependent on the applied magnetic field strength. Similar profile has been shown by Horowitz et al.<sup>15</sup> for an optic trap of NV defects oriented with isotropic density. To examine rotationally free characteristics of the particle in ABEL trap, we performed ESR experiments in the presence of static magnetic fields. Obtained measurements are consistent with the model (Figure 4) and demonstrate the possibility of sensing static magnetic fields in platforms where ABEL trap is compatible. Moreover, a recent work by Maclaurin et al.<sup>30</sup> on a free diffusing diamond nanocrystal as sensitive magnetometer for fluctuating and oscillating fields validates the ABEL trap approach for magnetic sensing in closed fluidic environment.

**Materials and Methods.** *Fluorescent Nanodiamond (FND).* Thirty nanometer big FNDs were produced by helium-ion irradiation and thermal annealing of type Ib diamond nanocrystallites followed by oxygen etching in air and surface functionalization.<sup>31</sup> FNDs were thoroughly washed and resuspended in water at 1 mg/mL concentration with single FND having approximately 10 NV centers. To minimize FNDs precipitation and agglomeration we sonicated the sample prior to each ABEL trapping experiment.

**RF Circuit.** The total Hamiltonian of the NV defect is given by<sup>32–34</sup>

$$H = D(s_z^2 - S(S+1)/3) + E(s_x^2 - s_y^2) + \gamma \vec{B} \cdot \vec{S} \\ + H_{\text{SI}} + H_{\text{I}}$$

where  $D$  and  $E$  are zero-field splitting (ZFS) parameters,  $\gamma$  is spin gyromagnetic factor,  $\vec{B}$  is vector magnetic field,  $H_{\text{SI}}$  is hyperfine coupling to the  $^{14}\text{N}$  nucleus (spin I), and  $H_{\text{I}}$  is the nuclear term. By neglecting the nuclear interaction and external magnetic field, only the ZFS term will be focused on. Owing to

its  $C_{3v}$  symmetry<sup>35</sup> the transverse parameter  $E = 0$  and the sublevels  $|m_s = 0\rangle$ ,  $|m_s = \pm 1\rangle$  are separated by the energy equivalent to the parameter,  $D = 2.87$  GHz (Figure 3a). In this case, a microwave source at the resonance frequency  $f = D$  will excite the optically populated  $|m_s = 0\rangle$  states to the  $|m_s = \pm 1\rangle$  states. As the NV centers in  $|m_s = \pm 1\rangle$  states have higher probability of undergoing intersystem crossing<sup>36</sup> (ISC), this control mechanism serves as the basis for optically detected magnetic resonance (ODMR).

In our setup, the green laser,  $\lambda = 561$  nm, used in ABEL trap for tracking operates also as optical pump for  $|m_s = 0\rangle$  states. The microwave excitation of these states has been realized using the enhanced magnetic field generated near the discontinuity on a coplanar waveguide transmission line (Figure 1d). This configuration was used for two reasons. First, all the conducting material is on the same surface of the dielectric that avoids the optic blockage. Second, the geometry does not require the presence of holes, which are difficult to realize on a thin cover glass. The enhancement of the field is due to evanescent or nonpropagating higher modes defined by the modified boundary conditions of the waveguide. The design of the CWG transmission line was accomplished using TXline and 3-D finite element analysis of the electromagnetic characteristics of the discontinuity carried out via COMSOL 4.2 RF Module.

**Kalman Filter.** The filter (Table 1) implemented for ABEL trap experiments is derived from the original algorithm<sup>37</sup> and

**Table 1. Kalman Filter Parameters Used in ABEL Trap Experiments**

update	predict
$(\gamma = p_{k/k-1}[p_{k/k-1} + 2w_0/n]^{-1})$	
$r_{k/k} = r_{k/k-1} + \gamma(EOD_{x,y} - x_{k-1/k-1})$	$r_{k/k-1} = r_{k-1/k-1} + \mu dt u_{k-1}$
$p_{k/k} = p_{k/k-1}(1 - \gamma)$	$p_{k/k-1} = p_{k-1/k-1} + 2Ddt$

the one used in the Cohen group.<sup>26</sup> The recursive nature of the filter enables a real time process using only present measurements and previously estimated parameters; full history of estimation is not required. The filter minimizes the mean of the squared error in the position estimation through predict and update steps.

Basically, there are two parameters propagating:  $r_{b/a}$  and  $p_{b/a}$  are the mean and variance estimates for the position of the particle at time  $b$  given all the data up to and including time  $a$ , respectively. The Kalman gain,  $\gamma$ , is the correcting factor for update step and scales the contributions of the measurements and the current state.  $EOD_{x,y}$  is the position of the rotating beam in the sample plane with beam size,  $2w_0$  (Supporting Information Figure S1).  $u$  is the feedback voltage vector where  $dt$  is the time period between the two consecutive update steps, and  $\mu$  and  $D$  are the electrokinetic mobility and the diffusion constant of the particle, respectively.  $\gamma$  is modeled such that it converges to unity when we have a very small beam waist size,  $w_0$ , leading to the higher resolution in scanning, and very large photon counts,  $n$ , which implies that the probability of hitting the molecule with the laser beam is at maximum. In this case, the update is determined by the laser position,  $r_{k/k} = EOD_{x,y}$ . While for the counter case ( $\gamma$  converges to zero) we do not trust the laser position, we use the previous estimates,  $r_{k/k} = r_{k-1/k-1}$  and  $p_{k/k} = p_{k-1/k-1}$ .

**Scanning Pattern.** The scanning pattern is generated through a rotating pencil-like Gaussian beam that is perpendicular to the sample plane. The beam waist  $w_0 \approx \lambda/\pi NA = 0.8 \mu\text{m}$  and  $2\pi w_0^2/\lambda \approx 7 \mu\text{m}$  were set via the focal length ratio of the scanner relay lenses (Figure 2a) controlling the radius of the collimated beam,  $w$ , entering the objective where  $NA \approx w/f_0$  is the numerical aperture,  $\lambda = 561 \text{ nm}$  is the operating wavelength, and  $f_0 = 3.33 \text{ mm}$  is the focal length of the objective (Nikon 60X PlanApo NA = 1.2). For optimal tracking, the rotating beam should cover the trap area and ensure that the molecule will be excited even if it is in the trap center. The radius of the trap area,  $R_0$ , is the parameter to control the intensity distribution of the rotating beam on the scanning plane (see Supporting Information Figure S1).

The intensity value of a point located at  $(x,y)$  is

$$I(x, y, t) = I_0 \exp[-2/w_0^2((x - x')^2 + (y - y')^2)]$$

where  $(x',y') = R_0(\sin(\Omega t), \cos(\Omega t))$ , is the instantaneous position of the Gaussian beam center at time  $t$ . The average value over one cycle is  $I(x,y) = I_0/2\pi \int_{-\pi}^{\pi} \exp[-2/w_0^2((x - x')^2 + (y - y')^2)] dt = I_0(4R_0r/w_0^2) \exp[-2(r^2 + R_0^2)/w_0^2]$  where  $I_0$  is the zeroth order of the modified Bessel function and  $r$  is the distance of the  $(x,y)$  point from the origin. The simulations (Supporting Information Figure S1) showed that the optimal scanning radius is  $R_0 \approx 0.7w_0$  since it provides both a uniform and large excitation area.

**RF Circuit Integrated Microfluidic Cell Fabrication.** Microfluidic channels in PDMS were molded on SU8 masters in multilayer form. A microfluidic depth of 800 nm in the trap center increases to 50  $\mu\text{m}$  toward the electrodes for electrical contact, confines the fields in the trap center, and suppresses resistive losses. Several outer rings were used to suppress the bias pressure (see Supporting Information). RF circuit on cover glass was formed through 200 nm of Cr and 800 nm of Al evaporation. After the electrical isolation with 30 nm of  $\text{Al}_2\text{O}_3$  the circuit was embedded in a PDMS layer of 4  $\mu\text{m}$  thickness to provide a flat surface for the microfluidics integration. The SMA connected chip then plasma bonded to the microfluidic cell with precise alignment under the microscope (see Supporting Information).

**Conclusions.** To summarize, here we demonstrated the position control and trapping of single FNDs using an ABEL trap that employs electrokinetic forces generated through the real-time particle tracking and its position estimation. Trapped single FND (30 nm in size) was optically excited with the same laser,  $\lambda = 561 \text{ nm}$ , used for the particle tracking. Microwave excitation of the spin states was performed using an RF circuit integrated to the trap platform. ESR spectrum upon the microwave excitation was detected, and it is in agreement with the previous observation on fixed or optically trapped nanodiamonds. In addition, we demonstrated that although ABEL trapped FNDs are subjected to the rotations, our device is sensitive enough to detect the presence of the static magnetic field. Given the fact that ABEL trap can already manipulate single rhodamine molecule, with the progress in the synthesis of the stable extremely small sized FNDs, we expect that our platform, in combination with the unique FND properties, opens up the possibility of performing a nanoscale magnetometry in closed fluidics environments.

## ■ ASSOCIATED CONTENT

### ■ Supporting Information

Supplementary methods with legends and additional references, Supplementary Figures 1–5, and Supplementary Movie. This material is available free of charge via the Internet at <http://pubs.acs.org>.

## ■ AUTHOR INFORMATION

### Corresponding Author

\*(M.K.) E-mail: metin.kayci@epfl.ch.

### Author Contributions

M.K. and A.R. designed the study. M.K. built ABEL trap, realized ESR setup, fabricated RF circuit integrated microfluidic devices, and performed COMSOL modeling and particle tracking on LabVIEW. M.K. performed all measurements and analyzed all data, presented in the letter and Supporting Information. M.K. prepared the manuscript. H.C.C. provided FNDs. A.R. supervised the project. All the authors read and commented on the manuscript.

### Notes

The authors declare no competing financial interest.

## ■ ACKNOWLEDGMENTS

Device fabrication was carried out in part in the EPFL Center for Micro/Nanotechnology (CMI). We thank Prof. Tobias Kippenberg (EPFL) and Alexey Feofanov (EPFL) for the use of the microwave generator. We thank Prof. Julien Perrisseau-Carrier (EPFL) for the discussion regarding design of RF circuits. We thank Prof. Adam Cohen (Harvard) for initial help with ABEL setup and LabVIEW software. We thank Prof. W. E. Moerner (Stanford) for discussion. This work was financially supported by the European Research Council (grant no. 259398; PorABEL, Nanopore integrated nanoelectrodes for biomolecular manipulation and design).

## ■ REFERENCES

- (1) Davies, G.; Hamer, M. F. *Proc. R. Soc. London, Ser. A* **1976**, *348* (1653), 285–298.
- (2) Gruber, A.; Drabenstedt, A.; Tietz, C.; Fleury, L.; Wrachtrup, J.; von Borczyskowski, C. *Science* **1997**, *276* (5321), 2012–2014.
- (3) Babinec, T. M.; Hausmann, B. J. M.; Khan, M.; Zhang, Y. A.; Maze, J. R.; Hemmer, P. R.; Loncar, M. *Nat. Nanotechnol.* **2010**, *5* (3), 195–199.
- (4) Englund, D.; Shields, B.; Rivoire, K.; Hatami, F.; Vuckovic, J.; Park, H.; Lukin, M. D. *Nano Lett.* **2010**, *10* (10), 3922–3926.
- (5) Maze, J. R.; Stanwick, P. L.; Hodges, J. S.; Hong, S.; Taylor, J. M.; Cappellaro, P.; Jiang, L.; Dutt, M. V. G.; Togan, E.; Zibrov, A. S.; Yacoby, A.; Walsworth, R. L.; Lukin, M. D. *Nature* **2008**, *455* (7213), 644–U41.
- (6) Taylor, J. M.; Cappellaro, P.; Childress, L.; Jiang, L.; Budker, D.; Hemmer, P. R.; Yacoby, A.; Walsworth, R.; Lukin, M. D. *Nat. Phys.* **2008**, *4* (10), 810–816.
- (7) Dolde, F.; Fedder, H.; Doherty, M. W.; Nobauer, T.; Rempp, F.; Balasubramanian, G.; Wolf, T.; Reinhard, F.; Hollenberg, L. C. L.; Jelezko, F.; Wrachtrup, J. *Nat. Phys.* **2011**, *7* (6), 459–463.
- (8) Neumann, P.; Jakobi, I.; Dolde, F.; Burk, C.; Reuter, R.; Waldherr, G.; Honert, J.; Wolf, T.; Brunner, A.; Shim, J. H.; Suter, D.; Sumiya, H.; Isoya, J.; Wrachtrup, J. *Nano Lett.* **2013**, *13* (6), 2738–2742.
- (9) Kucsko, G.; Maurer, P. C.; Yao, N. Y.; Kubo, M.; Noh, H. J.; Lo, P. K.; Park, H.; Lukin, M. D. *Nature* **2013**, *500* (7460), 54–U71.
- (10) Cuche, A.; Drezet, A.; Sonnefraud, Y.; Faklaris, O.; Treussart, F.; Roch, J. F.; Huant, S. *Opt. Express* **2009**, *17* (22), 19969–19980.

- (11) Balasubramanian, G.; Chan, I. Y.; Kolesov, R.; Al-Hmoud, M.; Tisler, J.; Shin, C.; Kim, C.; Wojcik, A.; Hemmer, P. R.; Krueger, A.; Hanke, T.; Leitenstorfer, A.; Bratschitsch, R.; Jelezko, F.; Wrachtrup, J. *Nature* **2008**, *455* (7213), 648–U46.
- (12) Degen, C. L. *Appl. Phys. Lett.* **2008**, *92*, 24.
- (13) Pauzauskie, P. J.; Radenovic, A.; Trepagnier, E.; Shroff, H.; Yang, P. D.; Liphardt, J. *Nat. Mater.* **2006**, *5* (2), 97–101.
- (14) Nakayama, Y.; Pauzauskie, P. J.; Radenovic, A.; Onorato, R. M.; Saykally, R. J.; Liphardt, J.; Yang, P. D. *Nature* **2007**, *447* (7148), 1098–U8.
- (15) Horowitz, V. R.; Aleman, B. J.; Christle, D. J.; Cleland, A. N.; Awschalom, D. D. *Proc. Natl. Acad. Sci. U.S.A.* **2012**, *109* (34), 13493–13497.
- (16) Geiselmann, M.; Juan, M. L.; Renger, J.; Say, J. M.; Brown, L. J.; de Abajo, F. J. G.; Koppens, F.; Quidant, R. *Nat. Nanotechnol.* **2013**, *8* (3), 175–179.
- (17) Svoboda, K.; Block, S. M. *Opt. Lett.* **1994**, *19* (13), 930–932.
- (18) Ashkin, A. *Proc. Natl. Acad. Sci. U.S.A.* **1997**, *94*, 4853–4860.
- (19) Cohen, A. E.; Moerner, W. E. *Appl. Phys. Lett.* **2005**, *86* (9), 093109.
- (20) Wang, Q.; Goldsmith, R. H.; Jiang, Y.; Bockenhauer, S. D.; Moerner, W. E. *Acc. Chem. Res.* **2012**, *45* (11), 1955–1964.
- (21) Fields, A. P.; Cohen, A. E. *Methods Enzymol.* **2010**, *475*, 149–174.
- (22) Cohen, A. E.; Moerner, W. E. *Proc. Natl. Acad. Sci. U.S.A.* **2007**, *104* (31), 12622–12627.
- (23) Wang, Q.; Moerner, W. E. *ACS Nano* **2011**, *5* (7), 5792–5799.
- (24) Goldsmith, R. H.; Moerner, W. E. *Nat. Chem.* **2010**, *2* (3), 179–186.
- (25) Bockenhauer, S.; Furstenberg, A.; Yao, X. J.; Kobilka, B. K.; Moerner, W. E. *J. Phys. Chem. B* **2011**, *115* (45), 13328–13338.
- (26) Fields, A. P.; Cohen, A. E. *Proc. Natl. Acad. Sci. U.S.A.* **2011**, *108* (22), 8937–8942.
- (27) Wang, Q.; Moerner, W. E. *J. Phys. Chem. B* **2013**, *117* (16), 4641–4648.
- (28) Rendler, T.; Renz, M.; Hammann, E.; Ernst, S.; Zarrabi, N.; Borsch, M. *Proc. SPIE* **2011**, *7902*, 79020M.
- (29) Mochalin, V. N.; Shenderova, O.; Ho, D.; Gogotsi, Y. *Nat. Nanotechnol.* **2012**, *7* (1), 11–23.
- (30) Maclaurin, D.; Hall, L. T.; Martin, A. M.; Hollenberg, L. C. L. *New J. Phys.* **2013**, *15*.
- (31) Fu, C. C.; Lee, H. Y.; Chen, K.; Lim, T. S.; Wu, H. Y.; Lin, P. K.; Wei, P. K.; Tsao, P. H.; Chang, H. C.; Fann, W. *Proc. Natl. Acad. Sci. U.S.A.* **2007**, *104* (3), 727–732.
- (32) Felton, S.; Edmonds, A. M.; Newton, M. E.; Martineau, P. M.; Fisher, D.; Twitchen, D. J.; Baker, J. M. *Phys. Rev. B* **2009**, *79* (7), 075203.
- (33) Smeltzer, B.; McIntyre, J.; Childress, L. *Phys. Rev. A* **2009**, *80* (5), 050302.
- (34) Steiner, M.; Neumann, P.; Beck, J.; Jelezko, F.; Wrachtrup, J. *Phys. Rev. B* **2010**, *81* (3), 035205.
- (35) Acosta, V. M.; Bauch, E.; Ledbetter, M. P.; Waxman, A.; Bouchard, L. S.; Budker, D. *Phys. Rev. Lett.* **2010**, *104* (7), 070801.
- (36) Acosta, V. M.; Bauch, E.; Jarmola, A.; Zipp, L. J.; Ledbetter, M. P.; Budker, D. *Appl. Phys. Lett.* **2010**, *97* (17), 174104.
- (37) Simon, D. *Optimal State Estimation: Kalman, H<sub>infinity</sub>, and Nonlinear Approaches*; John Wiley & Sons: New York, 2006.